

Mutations in *half baked*/E-cadherin block cell behaviors that are necessary for teleost epiboly

Donald A. Kane^{*,‡}, Karen N. McFarland[†] and Rachel M. Warga^{*}

Department of Biology, University of Rochester, Rochester, NY 14627, USA

^{*}Present address: Department of Organismal Biology and Anatomy, University of Chicago, 1027 East 57th Street, Chicago, IL 60637, USA

[†]Present address: University of Virginia Health Systems, Department of Pathology, 415 Lane Road, Charlottesville, VA 22908, USA

[‡]Author for correspondence (e-mail: ddke@mail.rochester.edu)

Accepted 29 December 2004

Development 132, 1105–1116

Published by The Company of Biologists 2005

doi:10.1242/dev.01668

Summary

Epiboly, the spreading of the blastoderm over the large yolk cell, is the first morphogenetic movement of the teleost embryo. Examining this movement as a paradigm of vertebrate morphogenesis, we have focused on the epiboly arrest mutant *half baked* (*hab*), which segregates as a recessive lethal, including alleles expressing zygotic-maternal dominant (ZMD) effects. Here we show that *hab* is a mutation in the zebrafish homolog of the adhesion protein E-cadherin. Whereas exclusively recessive alleles of *hab* produce truncated proteins, dominant alleles all contain transversions in highly conserved amino acids of the extracellular domains, suggesting these alleles produce dominant-negative effects. Antisense oligonucleotides that create specific splicing defects in the *hab* mRNA phenocopy the recessive phenotypes and, surprisingly, some of the ZMD phenotypes as well. In situ analyses show that during late epiboly *hab* is expressed in a radial gradient in the non axial epiblast, from high concentrations in the exterior

layer of the epiblast to low concentrations in the interior layer of the epiblast. During epiboly, using an asymmetric variant of radial intercalation, epiblast cells from the interior layer sequentially move into the exterior layer and become restricted to that layer; there they participate in subtle cell shape changes that further expand the blastoderm. In *hab* mutants, when cells intercalate into the exterior layer, they tend to neither change cell shape nor become restricted, and many of these cells ‘de-intercalate’ and move back into the interior layer. Cell transplantation showed all these defects to be cell-autonomous. Hence, as for the expansion of the mammalian trophoblast at a similar developmental stage, *hab*/E-cadherin is necessary for the cell rearrangements that spread the teleost blastoderm over the yolk.

Key words: Epiboly, Radial intercalation, E-cadherin, Epiblast, Teleost, Morphogenesis, Genetics, Antisense, Zebrafish

Introduction

Here we report on the molecular identity and the cellular basis for the epiboly defects in mutant alleles of the *half baked* (*hab*) locus, identified in the Tübingen large-scale genetic screen for mutations that affect morphogenesis in the zebrafish, carried out at the Max Planck Institut für Entwicklungsbiologie (Haffter et al., 1996). Epiboly is blocked in the mutants *hab^{div43}*, *lawine^{ts18}*, *avalanche^{tm94}*, *weg^{ts230}* and *volcano^{tm712}* (Kane et al., 1996; Solnica-Krezel et al., 1996). In all these mutants, epiboly begins and continues normally during the blastula and early gastrula stage. The first phenotypes are seen at 70 to 80% epiboly, about 1.5 to 2 hours after the onset of gastrulation, when the mutants begin to arrest their vegetalward spreading. Curiously, the enveloping layer, a thin epithelium that covers the deep cells of the blastoderm, and the syncytial layer of the yolk cell are unaffected and both complete epiboly normally; only the movements of the deep cells are arrested. Hence, the mutants demonstrate that some aspects of the epiboly of the deep cells are under a separate control from that of the enveloping layer and the yolk cell.

Additionally, three of the five epiboly mutants display dominant phenotypes. The mutants *hab^{div43}*, *avalanche^{tm94}* and *lawine^{ts18}* display a zygotic-maternal dominant (ZMD) effect

that is expressed when both zygotic and maternal genomes are heterozygous for the mutant locus. This phenotype is displayed as an intermediate rate of epiboly between that of wild-type and homozygous mutant siblings. These embryos, termed ZMD mutants, complete epiboly about an hour after wild-type siblings, and later, during somitogenesis, cells dorsal to the developing neural tube round up and detach from the embryo (Kane et al., 1996). Also, *hab^{div43}* mutants display a semi-dominant trait of an enlarged hatching gland.

Although the epiboly mutants failed to complement one another, they were named separately because complementation testing was complicated by the dominant effects. In recent work, submitted elsewhere, we have shown that all the mutants (with the exception of *vol*) map to a single locus near the centromere of Linkage Group 7, and the locus is provisionally named the *hab* locus. Here we establish that all of the mutations at the *hab* locus are in a single gene. Hence, all the alleles have been renamed *hab*, following the precedent for the nomenclature of *somitabun/captain hook* (Kramer et al., 2002), which also includes dominant and recessive alleles.

In the first portion of this work, we demonstrate that the alleles of *hab* are mutants in a single gene that encodes a zebrafish homolog of E-cadherin, an important membrane

protein necessary for homotypic cell adhesion (Takeichi, 1987). In the mouse, E-cadherin mRNA is present maternally and E-cadherin function is necessary for the process of cell compaction in the 8-cell stage embryo (Ao and Erickson, 1992). Later, as zygotic expression of E-cadherin begins, it is necessary for the expansion of the trophectoderm (Larue et al., 1994). In the zebrafish, E-cadherin mRNA is present maternally (Babb et al., 2001), and experiments based on antisense oligonucleotides have shown that E-cadherin is necessary for blastomere adhesion during the cleavage stage, and later for aspects of morphogenesis during gastrulation and epiboly (Babb and Marrs, 2004). In frogs, based on dominant negative analysis, E-cadherin seems more important for tissue integrity during early development (Heasman et al., 1994; Levine et al., 1994), whereas the closely related C-cadherin is necessary for morphogenesis (Lee and Gumbiner, 1995). However, the two cadherins overlap in their expression patterns and possibly functionally as well. In all creatures, during and after gastrulation, E-cadherin is expressed in the epidermal ectoderm, in a pattern complementary to the expression of N-cadherin in the neural ectoderm, and in the endoderm (Rutishauser et al., 1988; Takeichi, 1995). Later, reflecting its diverse role in numerous developmental and epithelial tissue functions, E-cadherin is also expressed in many epithelial tissues, including some that are mesodermally derived.

At the structural level, the protein is characterized by five extracellular cadherin (EC) repeats, a single pass transmembrane domain and a cytoplasmic domain. The EC repeats are extremely conserved among their homologs in other species, and are necessary for the specific adhesion properties of E-cadherin (Blaschuk et al., 1990). The cytoplasmic domain of the protein binds α - and β -catenin, and indirectly actin, simultaneously anchoring the protein to the cytoskeleton of the cell and connecting the molecule to the WNT signaling pathway (Gumbiner and McCrea, 1993; Herrenknecht et al., 1991; Kintner, 1992; McCrea et al., 1991; Sanson et al., 1996). The protein is thought to function as a dimer, and the EC repeats are necessary for this dimerization (Briehner et al., 1996; Nagar et al., 1996). This fact has been the basis for the creation of transgenes that abate gene function: deleting one or two of the exterior EC domains allows dimerization between mutant and wild-type E-cadherins, blocking E-cadherin function and causing a very effective dominant negative effect.

In the second portion of this work, we examine the role of *hab* in the morphogenesis of the epiblast during zebrafish epiboly, focusing on the differences in cell movement between *hab* mutants and wild-type embryos. The epiblast forms from all the deep cells of the blastoderm, and, somewhat similarly to the amniote epiblast, contributes cells to the hypoblast throughout gastrulation. Afterward, the epiblast forms the anlage for the ectodermal derivatives, whereas the hypoblast forms the anlage for mesodermal and endodermal derivatives. The epiblast thins as it spreads over the yolk cell, from about five cells thick at doming stage to about two cells thick at 100% epiboly, and finally to one cell thick in all but the axial region in the early segmentation stages. We hypothesized that this thinning may be due to the morphogenetic process of radial intercalation, the means where two or more layers of cells thin into a single layer, thus causing an expansion in surface area of the resulting layer. Using scanning electron micrographs of freeze-fractured blastulae, radial intercalation was classically

described in the amphibian blastocoel roof (Keller, 1980), and this process is thought to be a driving force for the expansion of the amphibian animal cap. Radial intercalation is also known to occur in the zebrafish blastula as the blastoderm thins during the doming stage, and is renowned for its annoying property of mixing blastula cell lineages, thus causing the indeterminate early fate map of zebrafish (Helde et al., 1994; Kimmel and Warga, 1987; Warga and Kimmel, 1990; Wilson et al., 1995). It is notable that in all the above examples, frog and fish, it is not clear if radial intercalation by itself is a force generating movement or if the movement is a passive response of a tissue to outside forces, e.g. being stretched or being compressed between two opposing tissues, as has been suggested by Wilson et al. (Wilson et al., 1995).

Here we describe the cell behaviors that drive late epiboly in the zebrafish embryo. We find two previously unrecognized layers in the zebrafish epiblast, the exterior layer of the epiblast and the interior layer of the epiblast, and we show that each of these layers have unique functions in this zebrafish version of radial interaction. In *hab* mutant embryos, these layers do not form completely and other cellular behaviors involved with radial intercalation do not occur normally. Finally, using cell transplantation, we show that the *hab* defects occur cell-autonomously, demonstrating that defects in radial intercalation are the most likely cause for the *hab* epiboly defect.

Materials and methods

Zebrafish strains

The *hab^{div43}*, *hab^{im94}*, *hab^{ts18}*, and *hab^{ix230}* alleles were isolated in a large-scale mutagenesis screen (Haffter et al., 1996) and initially out-crossed to the polymorphic WIK (L11) strain of wild-type fish for mapping. Subsequent generations were out-crossed to various wild-type strains of fish that were prescreened for polymorphisms in the appropriate microsatellite markers surrounding the *hab* locus. Fish carrying the *hab^{mut44}* allele were a gift from Dr Solnica-Krezel (Vanderbilt University). In this report, mutant embryos were always produced by mating two heterozygous parents. In the case of the ZMD alleles, this produced recessive mutants, ZMD mutants and wild-type embryos in a 1:2:1 ratio. Although there is a very slight maternal effect in the wild-type embryos produced from ZMD crosses, the phenotype is well within the variation seen in normal wild-type embryos.

Positional cloning of the *hab* locus

hab was initially mapped to the centromere of Linkage Group 7 by half tetrad analysis (Johnson et al., 1995). For fine-resolution mapping we used a panel of 2916 haploid embryos and identified two closely linked microsatellite markers on either side of the *hab* locus (Knapik et al., 1998). These markers were used to isolate clones from a large-insert genomic library (Amemiya et al., 1999) and construct a contig, as has been described (Wei and Malicki, 2002). Clones spanning the critical region of *hab* were sequenced as part of the ongoing Zebrafish Genome Project (GenBank Accession numbers: PAC18005: AL929461; PAC109L11: AL929295). To determine the site of the *hab* mutations we isolated total RNA from wild-type and *hab* embryo pools and generated E-cadherin cDNA by reverse transcription and PCR amplification using five overlapping primer pairs designed from the published cDNA sequence and compared sequence. We confirmed each mutation by isolating total RNA or genomic DNA from individual mutant and wild-type embryos to generate sequence for the site of lesion. Sequences of PCR primers are available from the corresponding author upon request.

hab morpholino oligonucleotides

hab/E-cadherin splice site-targeting morpholino oligonucleotides were designed from trace sequences deposited by Sanger before the draft sequence was available. Exons were identified by comparison of the mRNA sequence to the genomic sequence and numbered according to mouse terminology (Ringwald et al., 1991). Morpholinos were purchased from Gene Tools, the sequence of MO1 is: 5'-GTAACACACAGTAACCTTTACAGTGG-3'; and the sequence of MO2 is: 5'-AAGCATTCTCACCTCTCTGTCCAG-3'. We monitored splicing events by RT-PCR using pools of five embryos for each developmental timepoint. Sequences of PCR primers used for monitoring are available from the corresponding author upon request.

Embryo manipulations and genotypic characterization

For targeted gene-knockdown, we injected wild-type embryos with morpholino oligonucleotides (Gene-Tools) at the 1-cell stage. For transplants, we labeled donor embryos derived from crosses of *hab^{tm94}* heterozygotes with a mixture of 3% rhodamine-dextran and 3% biotin-dextran (Molecular Probes) at the 1- to 8-cell stage and transplanted donor cells into wild-type embryos at the onset of epiboly using standard procedures (Ho and Kane, 1990). Donor embryos were harvested and genotyped using the closely linked microsatellite marker Z20715 (F-5'-CATCTGTAAGTGCCAGCAA-3', R-5'-GTGTCCGGTTAGGCTACAAT-3'). Host embryos were fixed at 80% epiboly and processed as below for the co-injected biotin-dextran. For in vivo cell labeling, we injected a single superficial blastomere with 3% rhodamine-dextran at the 2k- to 4k-cell stage using standard procedures (Warga and Nüsslein-Volhard, 1999) in embryos derived from crosses of *hab^{dtv43}* heterozygotes. For these experiments we selected parental strains that gave less severe epiboly phenotypes so that survival of homozygous offspring persisted through the epiboly period. Embryos were genotyped by phenotype at the 100% epiboly stage based on the epiboly arrest trait of homozygous embryos and the detached cell trait of heterozygous embryos. Heterozygous embryos were reconfirmed at 24 hours by the enlarged hatching gland trait.

Immunohistochemistry and RNA in situ hybridization

Embryos injected with biotinylated-dextran were processed as described in the *Zebrafish Book* (Westerfield, 1993), cleared, mounted in Permout™ (Fischer Scientific) and photographed.

Antibody staining was carried out as described (Warga and Nüsslein-Volhard, 1999); briefly, embryos derived from either wild-type parents or *hab^{dtv43}* heterozygous parents were stained with anti-β-catenin (Sigma), embedded in 17% gelatin: 50% glycerol and bisected along the 90° meridian by hand using a razor blade. Afterward, these hand-sections were cleared, mounted in Permout and photographed.

RNA in situ hybridization was carried out as described (Thisse et al., 1993) using embryos derived from wild-type parents. Afterward, hand-sections were cut as described above, cleared in 70% glycerol and photographed.

Time-lapse and data analysis

For in vivo observations, embryos derived from *hab^{dtv43}* heterozygotes were mounted and recorded in multi-plane as previously described (Warga and Kane, 2003). Afterward, the recordings were analyzed using Cytos Software, looping half-hour segments from the time-lapse recording. In the case of Fig. 7, black and white images from one plane of the time-lapse video recording were imported into Adobe Photoshop and pseudo-colored to aid in presentation, matching the color of cells shown in the model in Fig. 9.

For analysis of cell shape, multiple planes from one time-lapse video segment were imported into Adobe Photoshop and reconstructed three-dimensionally so that individual cells in both the exterior and interior layer of the epiblast layer could be outlined as shown in Fig. 6. Both aspect ratio and cell surface area were calculated

by importing these outline images into NIH Image and running macro programs, as previously described in Warga and Kane (Warga and Kane, 2003).

For analysis of cell-autonomy, chimeras were cleared, mounted and the entire donor population recorded using a Zeiss Axiophot II equipped with a CDC-300-RC camera (Dage MTI) with a digital output to a Power Macintosh 9600/350. Images were then imported into Adobe Photoshop, reconstructed three-dimensionally and analyzed in NIH Video, as described above. For the analysis of cell restrictions in the exterior layer of the epiblast, we examined clones of cells in face view when embryos reached 75% epiboly using a Zeiss DIC 40× water immersion lens on a Zeiss Axioskop equipped with a Sony F-707 Digital Camera. Using the EVL layer as a reference, cell depth was determined by counting the number of cells between the surface and the labeled cell. Clones in and near the axis were excluded because of the more complex layering in the neural keel.

Results

The half baked mutations map to the gene encoding the zebrafish homolog of E-cadherin

Using microsatellite markers, we mapped *hab* to a 0.2 cM region near the centromere on Linkage Group 7 and, walking with overlapping P1-derived artificial chromosome (PAC) and bacterial artificial chromosome (BAC) clones (Amemiya et al., 1999), cloned the 500 kb region between flanking markers (Fig. 1). Clones that mapped within recombinants with *hab* were sequenced, revealing several cadherin-like sequences similar to the zebrafish homolog of E-cadherin cDNA (Babb et al., 2001). Further analysis showed severe rearrangements in the clones, which were probably artifacts that occurred in the library vectors or, in some cases, in the initial assembly of the sequence data. Nevertheless, one clone, PAC 71B9, contained the genomic sequence of zebrafish E-cadherin extending from exon3 to exon14.

All the *hab* alleles were sequenced from cDNA generated by RT-PCR (Fig. 2). Two of these alleles, *hab^{ts230}* and *hab^{mut44}*, were exclusively recessive and both contained nucleotide transversions that produced stop codons in the EC4 domain at amino acid positions 547 and 553, respectively. We noted in these experiments a reduction in the recovery of the RT-PCR product (data not shown), suggesting that nonsense-mediated transcript degradation was occurring. The other three alleles had ZMD effects. Two of these ZMD alleles, *hab^{tm94}* and *hab^{ts18}*, had mutations in the nucleotides that encoded the EC1 domain. In *hab^{tm94}*, the well-conserved valine¹⁶² was changed to an aspartic acid, and in *hab^{ts18}*, the well-conserved tyrosine¹⁷⁶ was changed to an asparagine. The third dominant allele, *hab^{dtv43}*, had an additional phenotype, a semi-dominant hatching gland enlargement trait; this allele possessed a mutation in the nucleotides that encoded the EC5 domain, changing the well-conserved isoleucine⁶⁰⁰ to a lysine.

Phenocopy of the dominant and recessive hab phenotypes using antisense oligonucleotides

To date, we have not completed the construction of an appropriate construct of *hab* to produce mRNA that could be used to rescue *hab* mutants. Therefore, to confirm that these mutations caused the *hab* phenotype, we injected antisense oligonucleotides into embryos to disrupt the zygotic gene function of *hab* and compared the knockdown phenotypes to that of *hab* mutants. Annealing antisense oligonucleotides to

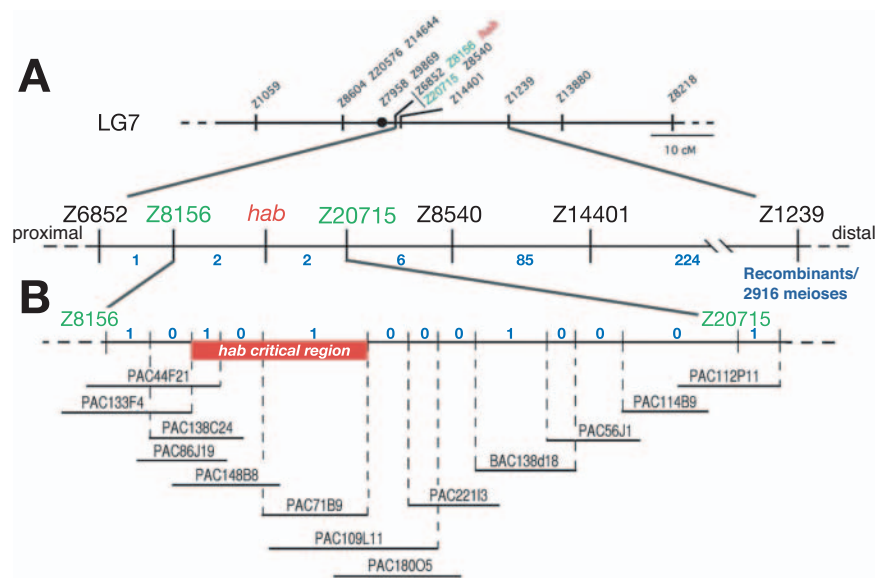


Fig. 1. Positional cloning of the *hab* locus. (A) Genetic map of the *hab* locus near the centromere (filled circle) of Linkage Group 7, showing the positions of the microsatellite (Z) markers and the number of recombinants between each marker. (B) The chromosomal walk was initiated at flanking markers Z20715 and Z8156, which were used to probe PAC and BAC large insert genomic libraries. Clones are numbered according to reference number (see Materials and methods). The critical region of 150 kb that contains *hab* was defined by the two closest recombination events. Sequencing of this region, as part of the Zebrafish Genome Project (Sanger Institute), revealed a number of candidate genes, including the zebrafish homolog of E-cadherin.

the splice donor site causes splicing defects, which in turn, disrupt specific regions of the protein product (Draper et al., 2001). Having no effect on already processed mRNAs, this approach knocks down the zygotic function of the targeted gene but not the maternally expressed mRNA product. Hence, the phenocopy should resemble the zygotic phenotype, not the potential maternal phenotype. The oligonucleotide MO1 (Fig. 3A) was designed to anneal with the exon9-intron9 junction. Embryos injected with MO1 produced a phenocopy that was very similar to the epiboly arrest of the *hab* recessive

phenotype (Fig. 3B). At reduced doses, the phenocopy became less extreme, similar to the slowing of epiboly in the ZMD mutants, and no additional phenotypes appeared in the surviving embryos. Sequencing the RT-PCR product after the experiment showed that intron9 found a cryptic donor site within exon9 at gt^{1329} , producing a small deletion in the mRNA (Fig. 3C). This caused a frameshift error upon entering exon10, and the conceptual protein (Fig. 3D) was truncated at stop codon in the downstream region of EC3, at approximately amino acid 420, a product 130 amino acids shorter than that predicted for the recessive *hab* alleles.

In a second experiment, the oligonucleotide MO2 was designed to target the exon7-intron7 junction. MO2 caused an extreme phenocopy of the *hab* recessive phenotype, displaying not only an epiboly arrest, but also causing the disaggregation of cells throughout the blastoderm (arrowhead in Fig. 3E), a phenotype often seen immediately before homozygous mutant embryos dissociate. At intermediate doses, we noticed that the blastoderm tended to thin unevenly before the epiboly arrest (arrow in Fig. 3E). At low doses, besides slowing epiboly, cells detached from the region dorsal of the neural tube, an aspect of the neural tube closure trait of the ZMD phenotype (Fig. 3E,F,G). Sequencing the knockdown product showed that MO2 caused an exon jump, producing a large in-frame deletion that removed all of exons 5 through 8 (Fig. 3H,I). In the conceptual protein, this resulted in a deletion from isoleucine¹⁶⁵ to glutamic acid³²², effectively removing the EC1 and EC2 domains of *hab* while leaving the signal sequence and pro domains intact, as well as the entire carboxy half of the protein. Thus, the MO2 protein product would be predicted to insert normally in the cell membrane but be lacking the function of the external EC domains of the protein, and may have similar effects to the dominant *hab*

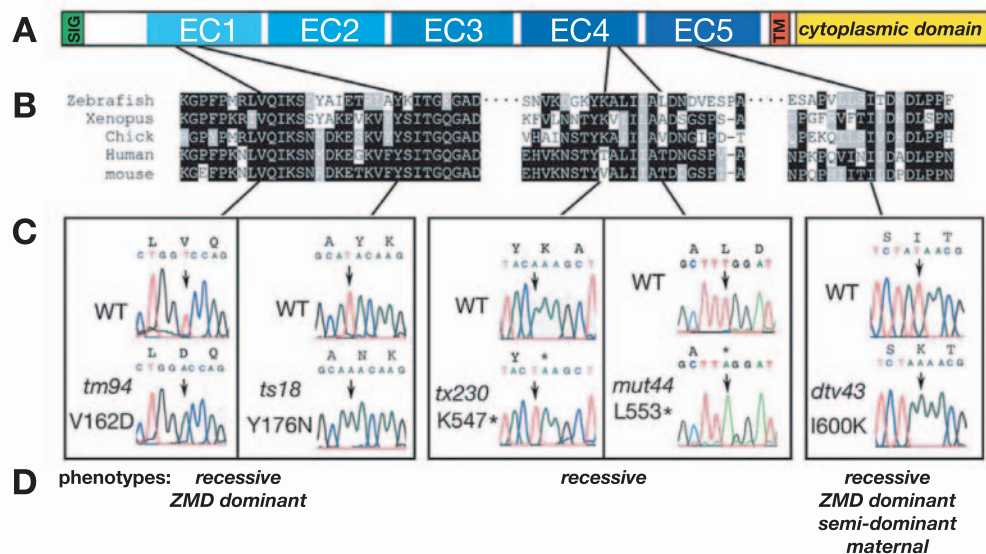
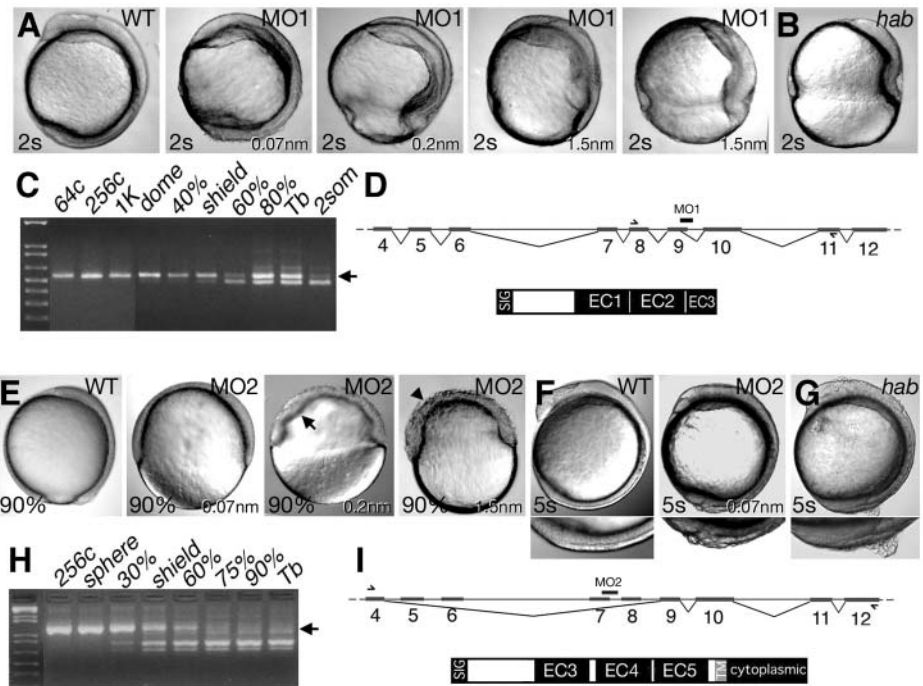


Fig. 2. *hab* encodes the zebrafish homolog of E-cadherin. (A) Domain structure of E-cadherin, showing signal sequence, and extracellular, transmembrane and cytoplasmic domains. (B) The zebrafish amino acid sequence for each local region containing a mutation and the corresponding amino acid sequence alignments for *Xenopus*, chick, human and mouse. Identical residues are black; conserved residues are gray. (C) Sequence trace data showing the site of each point mutation and the corresponding change in the amino acid sequence. (D) Mutations that fall in the same domain of the protein correlate with unique traits of the phenotype. EC, extracellular domain; SIG, signal sequence; TM, transmembrane domain.

Fig. 3. Phenocopies of *hab* allele-specific traits by disruption of EC1 or EC4. (A) Injection of morpholino oligonucleotide MO1 into wild-type embryos at increasing doses mimics the epiboly arrest phenotype. (B) Phenotype of *hab*^{dtv43/dtv43} at equivalent stage. (C) Aberrant splice products caused by MO1 appear at doming, shortly after the beginning of zygotic transcription (Kane and Kimmel, 1993). Arrow indicates maternal product. (D) Splicing event caused by MO1 (black bar) and conceptual protein, inferred by sequencing RT-PCR product using the primers indicated by arrows in exon8 and exon11. (E) Injection of MO2 into wild-type embryos at increasing doses causes a severe epiboly arrest, uneven radial intercalation (arrow) and dissociation of the blastoderm (arrowhead). (F) Injection of MO2 into wild-type embryos at low doses mimics the ZMD trait. Embryos are shown at the 5-somite stage and the detached cell region is shown beneath at higher magnification. (G) Phenotype of ZMD *hab*^{tm94/+}. (H) Splice products caused by MO2. (I) Splicing event caused by MO2 and the conceptual protein, as inferred by sequencing the RT-PCR product using the primers indicated in exon4 and exon12.



alleles that possess transversions in the amino acids of the EC1 domain.

A radial gradient of *hab* expression in the non axial blastoderm during epiboly

To analyze the distribution of the *hab* gene product, we performed whole-mount in situ hybridizations, focusing our investigation on the embryonic epiblast before and during late epiboly, the time when the epiboly arrest trait of the mutant is most strongly expressed. At this stage, the epiblast is sandwiched between the very thin epithelium of the EVL, and, on the inside of the embryo, the yolk cell or, if present, the hypoblast.

Using a probe made to the full-length *hab* cDNA sequence, we found that cleavage stage embryos expressed *hab* ubiquitously, showing that the mRNA was present maternally (Fig. 4A), as shown previously (Babb et al., 2001). At 30% epiboly, *hab* expression began to fade, revealing a very subtle radial gradient of expression (Fig. 4B) from the deepest layers of the blastoderm (lowest expression) to the superficial cells of the blastoderm (highest expression). By shield stage, the epiblast began to clear on the dorsal side of the embryo and the gradient became steeper elsewhere (Fig. 4C). At the same time, *hab* was strongly expressed in the entire EVL layer (Fig. 4C,D), forming a ring of expression around the nuclei of these thin epithelial cells. Expression was especially high in a subpopulation of EVL cells that become the forerunner cells. At 70% epiboly, *hab* expression was maintained on the lateral and ventral sides of the epiblast, and, within those regions, formed a steep radial gradient that was highest in the cells just beneath the EVL (Fig. 4E,F), and was absent in the yolk cell. Expression of *hab* was maintained in the EVL and cleared in the axial portion of the epiblast (Fig. 4F',G); interior to this zone of clearing, expression was seen in the anterior edge of

the hypoblast (Fig. 4F',G), as shown previously (Babb et al., 2001), and is presented as an ad hoc control to demonstrate the penetration of the whole-mount in situ probe.

Within these experiments, we also examined preliminary expression patterns of *hab* in the recessive mutants of the missense allele *hab*^{dtv43} and the nonsense allele *hab*^{tx230}. In *hab*^{dtv43} mutants (Fig. 4H), we found the *hab* transcript was upregulated. The pattern was similar to that of wild-type embryos (Fig. 4E), although expression seemed to be abnormally high in the axial mesoderm, posterior of the prechordal plate. We have not noticed any particular aspect of the mutant phenotype that correlates with this observation. In *hab*^{tx230} mutants (Fig. 4I), we found almost complete absence of transcript. This is consistent with our difficulty in recovery of RT-PCR product for sequencing this mutant, as mentioned above, and further corroborates the idea that nonsense-mediated transcript degradation is occurring in the premature stop codon alleles.

Identification of the exterior layer and interior layer of the epiblast

During the examination of the above in situ experiments, there seemed to be slight differences in cell morphology that correlated with the concentration of *hab* in the superficial and deep cell layers of the epiblast. After fixing homozygous mutant and wild-type embryos at 80 to 90% epiboly, staining to visualize the cell membranes, and sectioning the embryos, two distinct layers of the epiblast could be distinguished on the ventral and lateral sides of the embryo (Fig. 5). The exterior layer of the epiblast was epithelial-like, containing thin cuboidal cells that spread under, and perhaps against, the EVL. In between the exterior layer and the hypoblast, there was an interior layer of the epiblast, which consisted of disorganized cells that tended to be oriented with their long axis

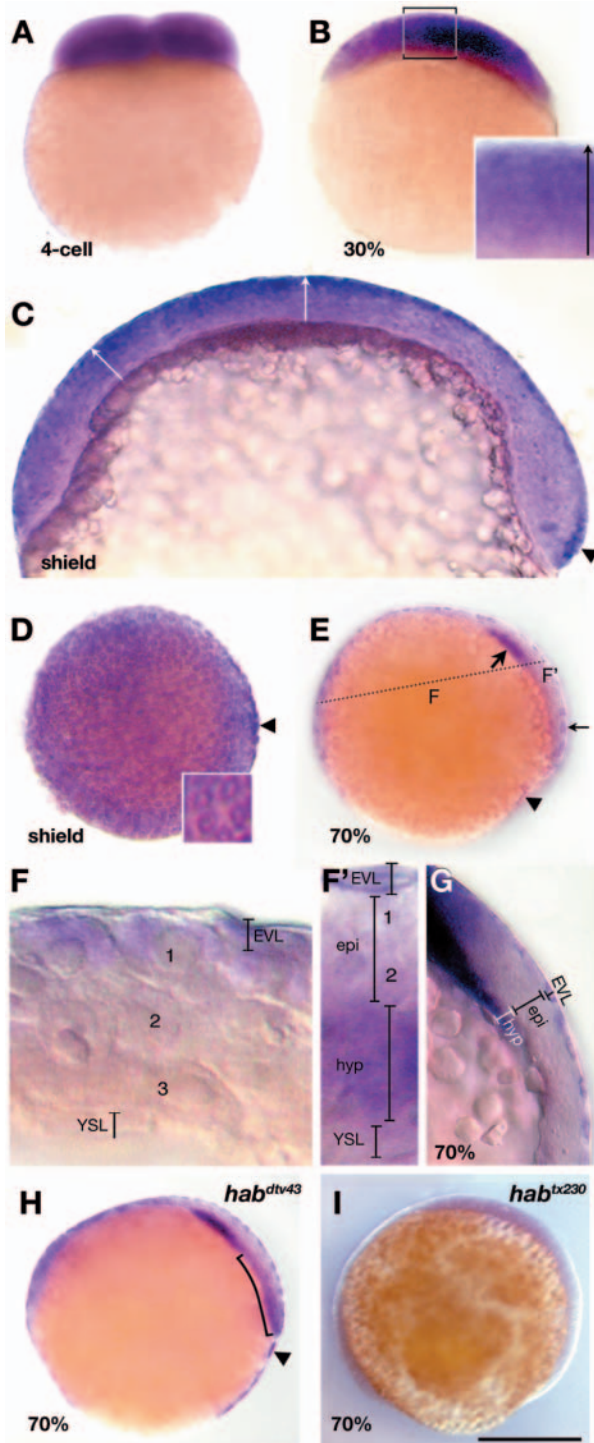


Fig. 4. Whole-mount in situ hybridization show that *hab* expression becomes progressively restricted to superficial layers of the blastoderm. (A) Optical cross-section of 4-cell stage. (B) Hand-section of 30% epiboly stage. Inset, higher magnification of boxed region showing a radial gradient (arrow) of *hab* expression in the epiblast, highest superficially. (C) Medial sagittal section of shield stage embryo, dorsal to the right. Arrows indicate the gradient of *hab* expression on the ventral side and at the animal pole. Note clearing on dorsal side, except for the thin line of expression in the EVL. Arrowhead indicates region of intense *hab* expression in the forerunner precursors. (D) Animal pole view of shield stage embryo showing high levels of *hab* expressed in the EVL, and the intense expression in the forerunner cells (arrowhead). Inset shows higher power view, showing nuclei surrounded by rings of *hab* expression. (E) Medial sagittal section at 70% showing high levels of *hab* expressed in the anterior axial hypoblast (thick arrow), the EVL (thin arrow), and the forerunner cells (arrowhead), and absence of *hab* expression in the axial epiblast. (F,F') High magnification views of embryo in E. Hand sections are along plane indicated by dashed line in E. (F) Lateral transverse section, showing a radial gradient of *hab* expression in the epiblast, highest in superficial layer adjacent to the EVL. At this location, the hypoblast has not yet moved under the epiblast. The numbers indicate approximate layers. (F') Dorsal transverse section, showing absence of *hab* expression in axial epiblast cells, and strong expression in anterior axial hypoblast near the level of the prechordal plate. At this stage, the midline of the neural epithelium is about two cells thick. (G) Medial sagittal section at 70% over stained to show the expression in the EVL, and the clearing in the axial epiblast. (H) Optical cross-section of 70% epiboly *hab*^{div43/div43} missense mutant showing raised levels of *hab* mRNA found in the blastoderm. Note intense expression in the forerunner clusters (arrowhead). Curved bracket indicates heightened expression in the hypoblast. Embryos in H and E are siblings. (I) Optical cross-section of 70% epiboly *hab*^{tx230/tx230} nonsense mutant showing lowered levels of *hab* mRNA found in the embryo. epi, epiblast; hyp, hypoblast; YSL, yolk syncytial layer. Numbers indicate cell layers of the epiblast. Scale bar: 100 μ m in C; 20 μ m in F,F'; 75 μ m in G; 250 μ m in all others.

be seen nicely in comparisons among homozygous mutants and wild-type embryos in Fig. 8).

Abnormal morphology of the epiblast layers in *hab* mutants is cell-autonomous

To quantitatively measure differences between *hab* mutant and wild-type embryos, we examined the area and aspect ratio of cells in optical sections of live embryos at 80 to 90% epiboly and found highly statistically significant differences between the exterior and interior layers of the epiblast. When viewed obliquely, cells of the exterior epiblast were spread out and displayed a high aspect ratio (Fig. 6A), which tended to align with the dorsal side of the embryo, as previously shown (Concha and Adams, 1998). By contrast, the cells of the interior layer of the epiblast, which had their long axes perpendicular to the surface of the embryo, displayed a small diameter with no aspect ratio in the plane parallel to the cell surface. In homozygous mutants (Fig. 6B), cells in the exterior layer of the epiblast had smaller apparent diameters, consistent with their being less spread out, and cells in the interior layer of the epiblast had larger diameters, consistent with their loss of a radial aspect ratio. Calculations of cell volumes showed no difference between the volumes of interior and exterior cells, or cells in mutant and wild-type embryos (data not shown).

perpendicular to the surface of the epiblast. In general, the border between the two layers was indistinct, and often individual cells were spanning the border. In homozygous *hab* mutants, cells in both layers were rounder than their wild-type counterparts: the cells of the exterior layer of the epiblast were less spread out, and the cells of the interior layer were less elliptical. Indeed, the mutant layers were so similar that it was difficult to say which layer contained the extra cells. Also, when compared with wild-type embryos, the exterior epiblast formed a less continuous epithelium in *hab* mutants (which can

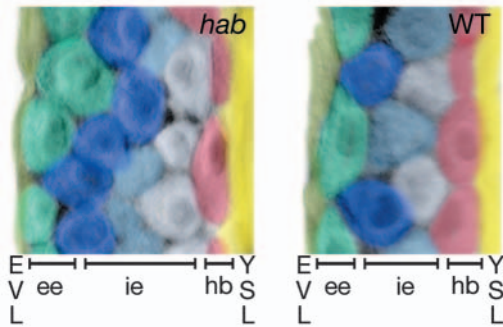


Fig. 5. Cell shape asymmetry and organization of the epiblast layer in *hab* mutants and wild-type embryos at 90% epiboly, showing Nomarski DIC photomicrographs of transverse sections of the lateral equator of fixed embryos stained with anti- β -catenin. Cells are pseudo-colored to distinguish cells and layers are labeled at the bottom of the figure. At this stage, the mesoderm is only one cell layer thick, and endoderm cells have moved out of the plane of the section (Warga, 1999). ee, exterior layer of the epiblast layer; hb, hypoblast layer; ie, interior layer of the epiblast layer; YSL, yolk syncytial layer.

To test the cell-autonomy of *hab*, we transplanted cells from homozygous mutant and wild-type siblings into the epiblast of wild-type hosts, and fixed the embryos at 80 to 90% epiboly. Examination of the morphology of the donor cells in the fixed material showed that cells from the mutant donors had strikingly identical sizes and aspect ratios to the measurements in the live mutants (Fig. 6C,D), demonstrating that the mutation acts cell-autonomously. We also noted the relative contributions from the homozygous mutant and wild-type donors to the exterior and interior layers of the host epiblast. Wild-type cells tended to contribute to the exterior layer of the epiblast (286 exterior:104 interior), whereas homozygous mutant cells did not (111 exterior:196 interior). Hence, although mutant cells are able to contribute to the exterior layer of the epiblast, they tend not to, and this bias is cell-autonomous.

Abnormal radial intercalation in *hab* mutants

We hypothesized that a combination of radial intercalation and cell shape changes drive the spreading of the blastoderm during epiboly. To directly observe these processes, we recorded homozygous mutant, ZMD mutant and wild-type siblings during late epiboly and documented occurrences of cells intercalating into – and out of – the exterior layer of the epiblast (Fig. 7). In ZMD mutants and wild-type embryos, as newly intercalated cells entered the exterior layer, they flattened to the dimensions typical of cells in that layer. This is shown for a ZMD *hab*^{div43/+} mutant in Fig. 7A. The process of entering the exterior layer and flattening typically took about 15 minutes and is shown in the supplementary material (Movies 1-3).

In homozygous mutants, cells from the interior layer also intercalated into the exterior layer (Fig. 7B), although the cells never completely flattened out. This process occurred somewhat quicker than in wild-type embryos, taking about 8 to 10 minutes. Surprisingly, in the homozygous mutants, exterior layer cells often returned to the interior layer (Fig. 7C). Examining time-lapse records over a 15 minute interval, we measured intercalation and de-intercalation events in

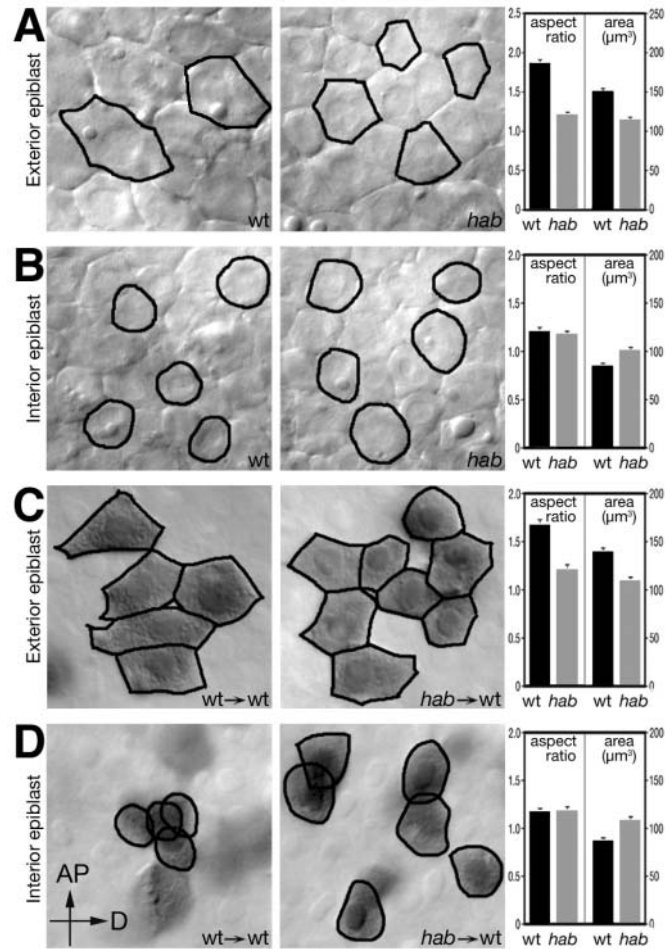


Fig. 6. Epiblast cells require *hab* to exhibit cell shape changes in a cell-autonomous manner. Optical sections through the exterior (A) and interior (B) layers of the epiblast of live wild-type and homozygous mutant *hab* embryos at 80% epiboly. Average aspect ratio (length/width) and surface area of wild-type and mutant cells were compiled from the outlines of cells (20-25 cells/embryo) for each layer in a total of three wild-type and four mutant embryos. Cell-autonomous effect of *hab* on cell shape in the exterior (C) and interior (D) layers of the epiblast. Wild-type or mutant cells were transplanted into the epiblast of a wild-type host and analyzed at the 80% epiboly stage. Transplanted cells are brown due to a fixable tracer. Data was compiled from outlines of donor cells (20-25 cells/host embryo) in a total of 15 chimeras, eight with cells from a wild-type donor and seven with cells from homozygous mutant *hab* donors. Note that aspect ratios and surface area of transplanted cells are almost identical to their live wild-type and mutant counterparts. Panels are orientated with the animal pole (AP) to the top and dorsal (D) to the right.

homozygous mutants, ZMD mutants and wild-type embryos (Table 1). De-intercalation events were never seen in wild-type embryos. However, in homozygous mutants, the rate of de-intercalation was almost equal to the rate of intercalation, suggesting that loss of the cells in the exterior layer of the epiblast is the physical basis for the arrest of epiboly. In ZMD mutants, there was approximately one de-intercalation event for every three or four intercalation events, which roughly correlates with the slowing of epiboly observed in the ZMD mutants.

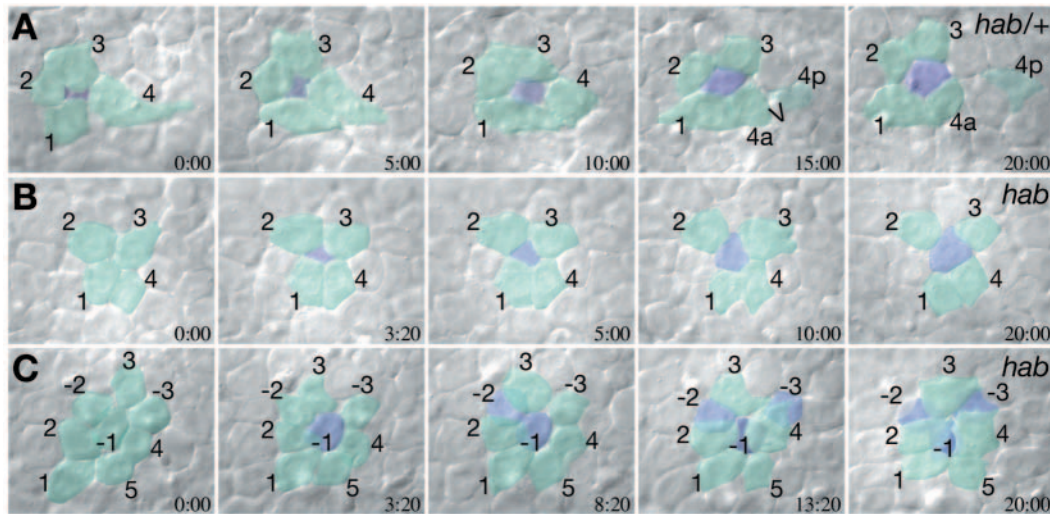


Fig. 7. Radial intercalation in heterozygous and recessive *hab* mutants. Selected frames from time-lapse video recordings of the lateral epiblast at about 80% epiboly using Nomarski DIC optics. Cells are pseudo-colored by layer and individual cells are identified by numbers. In both ZMD heterozygous (A) and homozygous *hab* mutants (B), cells from the interior layer of the epiblast (blue) intercalate in among cohorts of cells of the exterior layer (green). (C) In homozygous *hab* mutants, cells frequently leave the exterior layer. Three exterior cells (green with negative numbers), sequentially move to the interior layer of the epiblast (color shift to blue), and disappear under the neighboring exterior layer cells.

Cellular restrictions of the exterior layer of the epiblast

Following the evidence above, it seems that individual cells must enter the exterior layer of the epiblast (via radial intercalation), then change cell shape, and afterward they must become restricted to that layer. To test the restriction aspect of this hypothesis, we labeled individual cells near the animal pole when the blastoderm was at the 2000 to 4000 cell stage, shortly before the beginning of epiboly. Cells labeled in this period divided quickly over the next few hours, with the first division usually perpendicular to the plane of the surface, producing clonal descendents distributed between the EVL and the most superficial layer of the deep cell layer. Because cells of the EVL are restricted after the beginning of epiboly (Kimmel et al., 1990), they were disregarded for the remainder of the analysis. In other experiments, started slightly later, we labeled deep cells directly. At 80% epiboly, we examined the clones, counting the cells in the exterior layer of the epiblast and the approximate first and second interior layers. In general, clone sizes were about eight cells per embryo, and there was no difference in cell division between clones in mutant and wild-type embryos. Clones in wild-type embryos tended to

the epiblast normally remain in that layer throughout epiboly, and in mutant embryos, they do not.

Discussion

Based on identification of the mutant sequence and reproduction of the mutant phenotype with antisense oligonucleotides, we have shown that *hab* encodes the zebrafish homolog of E-cadherin. Here we discuss the nature of the mutations of *hab*. Then we consider the cellular behaviors that drive epiboly of the epiblast, which when disrupted, cause the *hab* phenotype.

The recessive alleles of *hab* act as nulls for zygotically expressed E-cadherin

The cell membrane protein E-cadherin requires the function of five EC domains, which facilitate the homophilic binding among cells, and a cytoplasmic portion necessary for interactions with the cytoskeleton. The recessive alleles of *hab* and the MO1 antisense oligonucleotide knockdown product all result in truncated proteins due to premature stop codons in the EC3 or EC4 domains. These mutations should produce

Table 1. Rates of intercalation in *hab* and wild-type embryos

Genotype*	Number of cells [†] (number of embryos)	Intercalation events [‡]	De-intercalation events	Rate [§] of intercalation	Rate of De-intercalation
<i>hab</i> ^{-/-}	435 (3)	41	35	37.7/100 h ^{1/2}	32.2/100 h ^{1/2}
ZMD <i>hab</i> ^{+/+}	326 (3)	27	8	33.1/100 h ^{1/2}	9.8/100 h ^{1/2}
Wild-type	321 (3)	29	0	36.1/100 h ^{1/2}	<0.6/100 h ^{1/2}

*All embryos are siblings from a single cross, *hab*^{dtv43/+} × *hab*^{dtv43/+}.

[†]Total number of cells at the beginning of the recording.

[‡]Events measured over a 15 minute interval at approximately 75% epiboly stage.

[§]Rates calculated as events per 100 cells per hour; The s.e.m. is $\pm 6/100$ h^{1/2}.

remain in the exterior layer of the epiblast (Fig. 8A,E). Some cells were found in the interior layers, but because we did not follow the cells, e.g. by time-lapse analysis, we do not know when they entered that layer. It must have been quite early, because in our analysis during late epiboly (Table 1), we never saw wild-type cells leaving the exterior layer. Clones in homozygous mutant embryos tended to be found equally in all layers of the epiblast (Fig. 8C,D,E), and clones in ZMD mutants showed distributions intermediate between the homozygous mutant and wild-type embryos (Fig. 8B,E). Therefore, notwithstanding cells that are lost to the hypoblast, cells of the exterior layer of

proteins that contain the signal sequence and the pro domain and the first two or three EC domains, but lack the inner EC domains, the transmembrane domain and the cytoplasmic portion of the protein. Hence, we imagine that the *hab* recessive alleles are functional nulls. Interestingly, both of the *hab* recessive alleles were truncated in EC4, similar to two of the three recessive alleles of *parachute* (*pac*), which encodes the zebrafish homolog of N-cadherin (Lele et al., 2002); these *pac* alleles are thought to be recessive nulls. Nevertheless, in the cases of either *hab* or *pac*, it is possible that the truncated protein products are secreted and have some unknown function.

Even if null, probably none of the *hab* phenotypes display the lack-of-function phenotype of the gene, for *hab* is maternally supplied. The lack-of-function phenotype may resemble the knockdown phenotype of using 5' antisense oligonucleotides seen by Babb and Marrs (Babb and Marrs, 2004), which should knock down maternal mRNA expression, or the phenotype could be more severe.

The ZMD alleles of *hab* act as dominant negatives

Our interpretation of the dominant phenotypes is that they are caused by mutations acting as antimorphic alleles. It is thought that cadherins act as dimers, and the EC repeats are necessary for dimerization (Briehner et al., 1996; Nagar et al., 1996; Takeda et al., 1999). Based on sequence analysis, all the dominant alleles and the MO2 antisense knockdown product should produce proteins that are properly inserted into the cell membrane of the cells that normally express wild-type *hab*, but possess one or more nonfunctional EC domains. These mutant proteins should dimerize with wild-type proteins, and thus interfere with gene function in a dominant negative fashion.

The dominant negative effects of the ZMD alleles are consistent with the strengths and behaviors of their phenotypes. First, in the case of heterozygous embryos derived from a wild-type mother and a father heterozygous for a ZMD allele, there is no dominance. In this case, we imagine that the maternally encoded protein is capable of competing the effect of the one zygotic copy of the dominant allele. By this argument, *hab* is the strongest of the dominant alleles, as it alone has a dominant effect in the absence of a heterozygous mother. Second, when homozygous, the dominant alleles express more severe epiboly defects than the recessive alleles of *hab* (Kane et al., 1996). Here we imagine that the zygotic products of the dominant allele partially inactivate the maternally supplied products, and

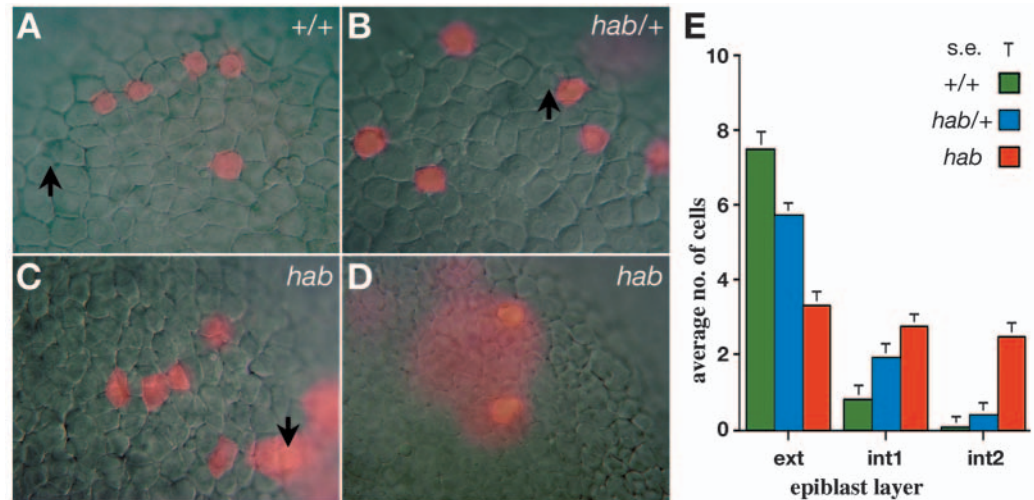


Fig. 8. Epiblast cells require *hab* to maintain superficial positions in the epiblast. Progeny of a single superficial cell labeled near the animal pole at the 4000-cell stage visualized at 80% epiboly in live homozygous mutants, ZMD mutants and wild-type siblings. (A) Clone in a wild-type embryo, in which all epiblast cells are located in the exterior layer. Note epithelial cell morphology of unlabeled cells. (B) Clone in a ZMD mutant, in which all epiblast cells are located in the exterior layer. (C) Rare clone in a homozygous *hab* mutant, in which the majority of epiblast cells are located in the exterior layer. Note the loose cell morphology of unlabeled cells. (D) Typical clone in a homozygous *hab* mutant, in which the majority of epiblast cells are located in the interior layer. (E) Distribution of clonal progeny in the epiblast layers of homozygous mutants, ZMD mutants and wild-type embryos. Arrows indicate examples of the large nuclei of EVL cells; diffuse staining (in D) is from thin cells of the EVL portion of the clone.

the phenotype is shifting toward what we would imagine is the maternal phenotype.

In the case of the ZMD alleles, the location of the mutation within the protein correlates with specific aspects of the dominant phenotypes, suggesting that domains of the protein may possess different functions in different regions of the embryo. For example, both *hab^{ts18}* and *hab^{im94}* possess

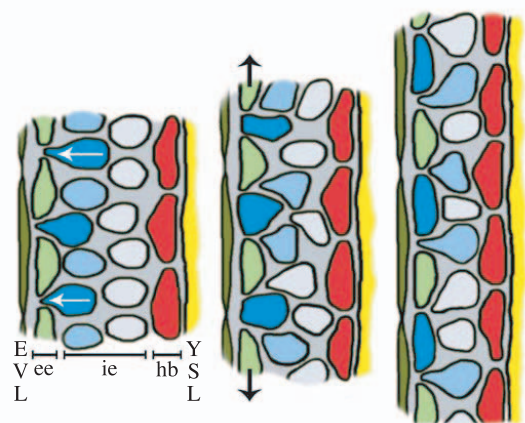


Fig. 9. Asymmetric radial intercalation and cell shape changes of the epiblast layer drive epibolic expansion of the lateral and ventral blastoderm of the zebrafish. Cells of the interior layer of the epiblast (blue, light blue, white) sequentially intercalate between the cells of the exterior layer (light green) and then flatten; arrows indicate directions of cell movement. Hypoblast cells (red) and EVL cells (dark green) move independently of the epiblast. ee, exterior layer of the epiblast; hb, hypoblast layer; ie, interior layer of the epiblast; YSL, yolk syncytial layer.

mutations in the EC1 domain, and both their ZMD neural tube phenotypes look very similar. Both phenotypes express defects focused in the tail, and there, the defects are severe. However, the *hab^{div43}* allele possesses a mutation in the EC5 domain. Its ZMD neural tube phenotype is expressed the entire length of the neural axis, but, in general, the effect is not locally severe. Moreover, the *hab^{div43}* allele has the dominant hatching gland defect; *hab^{tm94}* and *hab^{ts18}* do not. Interestingly, the one *pac* allele that is reported to possess some dominant effects is a missense mutant in EC1 of N-cadherin (Malicki et al., 2003). This particular mutant also has allele-specific phenotypes, expressing a more severe phenotype in the eye than the recessive *pac* alleles.

In humans, gastric cancers that are particularly invasive have been traced to familial inherited mutations in E-cadherin (Hajra and Fearon, 2002), and some of these mutations are transversions that result in amino acid substitutions in the EC1 and EC5 domains. Many of our fish lines that carry the *hab* dominant alleles show reduced long-term survival, and it will be of interest to examine the fish that survive only to early adulthood.

A model for expansion of the epiblast in the zebrafish embryo

Our results suggest that a combination of radial intercalation with other cell behaviors drive the spreading of the non-axial epiblast during late epiboly. We have shown the existence of two cell layers in the epiblast, which we term the 'exterior layer' and 'interior layer' (Fig. 9). Closely opposed to the well-organized epithelium of the EVL, cells of the exterior layer formed a continuous layer that roughly resembled a cuboidal epithelium. Underlying the exterior layer was the interior layer, a somewhat disorganized multilayer consisting of cells that tended to be aligned in a radial direction. Here we have documented that the cells of the interior layer of the epiblast moved into the exterior layer via radial intercalation. Once there, cells of the exterior layer tended to remain in the exterior layer, and became restricted to that layer.

We propose that the expansion of the epiblast has three components: first, cells of the interior layer radially intercalate into the exterior layer; second, the cells flatten as they join the epithelium of the exterior layer; third, these cells become restricted to the exterior layer.

Biomechanically, the model spreads the epiblast by two means. First, the process of radial intercalation increases the number of cells in the exterior layer of the epiblast, and thus expands the surface area of the epithelium, similar to the effect of radial intercalation in amphibians. Note that to secure this effect the cells should not leave the exterior layer. Second, the flattening of the cells further increases the surface area of the exterior epiblast. It is of interest that the exterior layer of the epiblast appeared to spread out against the EVL, as a substrate of sorts. Whereas this attachment was quite weak, for the epiblast freely slid under the EVL, the subtle interactions between the two layers might have mechanical consequences that are underappreciated.

The expansion of the zebrafish epiblast seemed to show a remarkable blend of *Xenopus* and mouse morphogenesis. The cell shape changes reported here for the exterior layer of the epiblast during teleost epiboly appeared very similar to those thought to occur during the expansion of the trophoderm

epithelium (Barcroft et al., 1998; Fleming et al., 2001; Reima et al., 1993). Based on morphogenetic arguments, the formation of the mammalian trophectoderm and the epiboly of the teleost blastoderm over the yolk have been suggested to be similar events (Kane and Adams, 2002). Interestingly, both these structures fail to form normally after zygotic E-cadherin is abrogated by mutation in either species (Kane et al., 1996; Larue et al., 1994), demonstrating that they are among the first structures that require the zygotic expression of E-cadherin. Observations such as these open questions as to the homology of these two structures.

Compared with radial intercalation in other model systems, teleost radial intercalation displays a number of unique differences. First, teleost epiboly may involve substrates, such as the EVL, that could organize radial intercalation. In urodeles, with the underlining of the animal cap by the void of the blastocoel, all the cell layers of the animal cap appear to participate equally in radial intercalation (Keller and Shook, 1994), resulting in a single layer at the completion of the process, and demonstrating that radial intercalation can be a substrate-free process. In this regard, zebrafish may have some similarities to *Xenopus*, which also possesses an outer epithelial layer that does not participate in radial intercalation (Keller, 1980). Second, teleost epiboly is markedly asymmetric. In amphibians, and especially in urodeles, there is an impression of two or three somewhat similar layers merging into a single epithelium. In teleosts, the exterior and the interior layers of the epiblast appear very different from one another. On the one hand, the exterior layer acts as a sink for the intercalation of cells and participates in cell shape changes, both processes that act to drive the epiblast over the yolk cell. On the other hand, the interior layer acts only as a reservoir, contributing cells as needed to the exterior layer. Such a mechanism might be more appropriate for teleost epiboly, where a relatively small but solid blastoderm must cover the huge yolk cell.

hab is necessary for restrictions and cell shape changes in the epiblast

Almost all the cell behaviors described by the above model exhibit defects in *hab* mutants. First, distinguishable exterior and interior layers of the epiblast did not form in the mutant. The cells of what would be the exterior layer fail to flatten and never form a continuous epithelium, and albeit more subtly, the cells of the interior layer failed to attain a radial aspect ratio. Second, radial intercalation in the mutant was negated by the inability of the cells to remain in the exterior layer. This aberrant cell movement was probably the direct cause for the arrest of epiboly.

The transplantation experiments demonstrate that *hab* acts in a cell-autonomous fashion. Hence, *hab* function is necessary within the cells themselves for their participation in the cell behaviors of the epiblast. More importantly, when mutant cells are placed in a wild-type embryo, both the cell shape phenotype of *hab* and the inability of *hab* cells to remain restricted to the exterior layer are virtually identical to the behavior of cells in mutant embryos. This result strongly indicates that the *hab* defects in cell behavior are not the result of other morphogenetic processes in the epiblast. We note that an important control experiment has not yet been done: that is, placing wild-type cells in mutant embryos. This experiment

would test whether wild-type cells can undergo normal cell behaviors in an embryo devoid of any global clues or forces that may be necessary for such cell behaviors, a non-autonomous effect. We had poor success with this experiment because of the general lethality of *hab* host embryos, which seems to be exacerbated by the process of transplantation itself. However, in other experiments, submitted elsewhere, we have seen that when wild-type cells are transplanted into neural tubes of ZMD mutants, the wild-type cells often assume mutant phenotype, suggesting that in certain situations, *hab* can act in a non-autonomous fashion. We are now breeding lines of the mutant *hab^{lx230}*, which has the least severe epiboly phenotype, in order to produce a recessive mutant that reliably survives into early segmentation stages.

Our observations regarding the radial concentration gradient of *hab* mRNA are in line with the defects observed in *hab* mutants. *hab* mRNA is expressed in the exterior layer of the epiblast, and that layer is missing in *hab* mutants. Possibly, cells of the exterior layer require additional *hab* gene product because they are forming an epithelium, and if they are unable to produce additional gene product, they do not integrate into the exterior layer and slip back into the interior layer. The radial gradient could also control the ordering and layering of cells during epiboly. Cells sort into layers dependent on adhesive activity (Duguay et al., 2003; Steinberg and Takeichi, 1994). One could imagine that as the blastoderm thins, cells with the highest concentration of *hab* gene product would move to the outside, against the EVL, which continuously expresses high levels of *hab* mRNA; cells with low concentrations would move to the yolk cell, which has downregulated *hab* mRNA. Indeed, in the MO2 antisense knockdown experiment we observed unevenness in the thicknesses of the blastoderm. Antisense injections are known to mix unevenly in the early cleavage embryo, and irregularities in oligonucleotide concentration would cause local differences in *hab* function. Hence, because cells would tend to adhere differently in regions of differing *Hab* concentrations, some regions would tend to be thicker than others.

In *hab* mutants, cells move, but many tissues do not. For example, radial intercalation occurs at the same rate in *hab* mutants as in wild-type embryos, but the mutant cells deintercalate, unable to remain in the exterior epiblast, and the epiblast ceases movement. In work to be presented elsewhere, we have found that many aspects of global convergence are affected in *hab* mutants, but the cells themselves continue to move at the same rate as cells in wild-type embryos. *Hab* seems specifically required for the normal integration of cells into embryonic epithelia and continues to be required for the normal behavior of the cells within the epithelia. Hence, in *hab* mutants, such epithelia form poorly or not at all; when they do form, the epithelia behave abnormally, causing the slowing or arrest of large-scale movements. Unraveling the roles that *Hab* and other molecules play in these early cell interactions that bind together the cells of the gastrula will be instructive, as we untangle these subtle forces that act to shape the vertebrate embryo.

We thank Dr Paul Myers for help on time-lapse analysis, Dr Sam Schlagman for help with construction of in situ probes, Dr John Postlethwait and Dr Angel Amores for advice on the chromosome work, and Dr Lila Solnica-Krezel for allowing the analysis of the

hab^{mu44} allele. We also thank the members of our laboratory and our colleagues at the University of Rochester, both those in the Medical Center and on Campus, for many helpful discussions. The Research was supported by grants from the Pew Charitable Trust and the National Institutes of Health to D.A.K.

Supplementary material

Supplementary material for this article is available at <http://dev.biologists.org/cgi/content/full/132/5/1105/DC1>

References

- Amemiya, C. T., Zhong, T. P., Silverman, G. A., Fishman, M. C. and Zon, L. I. (1999). Zebrafish YAC, BAC, and PAC genomic libraries. In *Methods in Cell Biology*, Vol. 60 (ed. W. Detrich, M. Westerfield and L. Zon), pp. 235-258. New York: Academic Press.
- Ao, A. and Erickson, R. P. (1992). Injection of antisense RNA specific for E-cadherin demonstrates that E-cadherin facilitates compaction, the first differentiative step of the mammalian embryo. *Antisense Res. Dev.* **2**, 153-163.
- Babb, S. G. and Marrs, J. A. (2004). E-cadherin regulates cell movements and tissue formation in early zebrafish embryos. *Dev. Dyn.* **230**, 263-277.
- Babb, S. G., Barnett, J., Doedens, A. L., Cobb, N., Liu, Q., Sorkin, B. C., Yelick, P. C., Raymond, P. A. and Marrs, J. A. (2001). Zebrafish E-cadherin: expression during early embryogenesis and regulation during brain development. *Dev. Dyn.* **221**, 231-237.
- Barcroft, L. C., Hay-Schmidt, A., Caveney, A., Gilfoyle, E., Overstrom, E. W., Hyttel, P. and Watson, A. J. (1998). Trophectoderm differentiation in the bovine embryo: characterization of a polarized epithelium. *J. Reprod. Fertil.* **114**, 327-339.
- Blaschuk, O. W., Sullivan, R., David, S. and Pouliot, T. (1990). Identification of a cadherin cell adhesion recognition sequence. *Dev. Biol.* **139**, 227-229.
- Briehier, W. M., Yap, A. S. and Gumbiner, B. M. (1996). Lateral dimerization is required for the homophilic binding activity of C-cadherin. *J. Cell Biol.* **135**, 487-496.
- Concha, M. L. and Adams, R. J. (1998). Oriented cell divisions and cellular morphogenesis in the zebrafish gastrula and neurula: a time-lapse analysis. *Development* **125**, 983-994.
- Draper, B. W., Morcos, P. A. and Kimmel, C. B. (2001). Inhibition of zebrafish *fgf8* pre-mRNA splicing with morpholino oligos: a quantifiable method for gene knockdown. *Genesis* **30**, 154-156.
- Duguay, D., Foty, R. A. and Steinberg, M. S. (2003). Cadherin-mediated cell adhesion and tissue segregation: qualitative and quantitative determinants. *Dev. Biol.* **253**, 309-323.
- Fleming, T. P., Sheth, B. and Fesenko, I. (2001). Cell adhesion in the preimplantation mammalian embryo and its role in trophectoderm differentiation and blastocyst morphogenesis. *Front. Biosci.* **6**, D1000-D1007.
- Gumbiner, B. M. and McCreary, P. D. (1993). Catenins as mediators of the cytoplasmic functions of cadherins. *J. Cell Sci. Suppl.* **17**, 155-158.
- Haffter, P., Granato, M., Brand, M., Mullins, M. C., Hammerschmidt, M., Kane, D. A., Odenthal, J., van Eeden, F. J., Jiang, Y. J., Heisenberg, C. P. et al. (1996). The identification of genes with unique and essential functions in the development of the zebrafish, *Danio rerio*. *Development* **123**, 1-36.
- Hajra, K. M. and Fearon, E. R. (2002). Cadherin and catenin alteration in human cancer. *Genes Chromosomes Cancer* **34**, 255-268.
- Heasman, J., Ginsberg, D., Geiger, B., Goldstone, K., Pratt, T., Yoshida-Noro, C. and Wylie, C. (1994). A functional test for maternally inherited cadherin in *Xenopus* shows its importance in cell adhesion at the blastula stage. *Development* **120**, 49-57.
- Helde, K. A., Wilson, E. T., Cretekos, C. J. and Grunwald, D. J. (1994). Contribution of early cells to the fate map of the zebrafish gastrula. *Science* **265**, 517-520.
- Herrenknecht, K., Ozawa, M., Eckerskorn, C., Lottspeich, F., Lenter, M. and Kemler, R. (1991). The uvomorulin-anchorage protein alpha catenin is a vinculin homologue. *Proc. Natl. Acad. Sci. USA* **88**, 9156-9160.
- Ho, R. K. and Kane, D. A. (1990). Cell-autonomous action of zebrafish *spt-1* mutation in specific mesodermal precursors. *Nature* **348**, 728-730.
- Johnson, S. L., Africa, D., Horne, S. and Postlethwait, J. H. (1995). Half-tetrad analysis in zebrafish: mapping the *ros* mutation and the centromere of linkage group I. *Genetics* **139**, 1727-1735.

- Kane, D. and Adams, R.** (2002). Life at the edge: epiboly and involution in the zebrafish. In *Gastrulation Movements*. Vol. 40 (ed. L. Solnica-Krezel), pp. 117-135. Heidelberg: Springer-Verlag.
- Kane, D. A. and Kimmel, C. B.** (1993). The zebrafish midblastula transition. *Development* **119**, 447-456.
- Kane, D. A., Hammerschmidt, M., Mullins, M. C., Maischein, H. M., Brand, M., van Eeden, F. J., Furutani-Seiki, M., Granato, M., Haffter, P., Heisenberg, C. P. et al.** (1996). The zebrafish epiboly mutants. *Development* **123**, 47-55.
- Keller, R. E.** (1980). The cellular basis of epiboly: an SEM study of deep cell rearrangement during gastrulation in *Xenopus laevis*. *J. Embryol. Exp. Morphol.* **60**, 201-234.
- Keller, R. and Shook, D.** (1994). Gastrulation in amphibians. In *Gastrulation, From Cells to Embryos* (ed. C. D. Stern), pp. 171-203. Cold Spring Harbor, NY: Cold Spring Harbor Laboratory Press.
- Kimmel, C. B. and Warga, R. M.** (1987). Indeterminate cell lineage of the zebrafish embryo. *Dev. Biol.* **124**, 269-280.
- Kimmel, C. B., Warga, R. M. and Schilling, T. F.** (1990). Origin and organization of the zebrafish fate map. *Development* **108**, 581-594.
- Kintner, C.** (1992). Regulation of embryonic cell adhesion by the cadherin cytoplasmic domain. *Cell* **69**, 225-236.
- Knapik, E. W., Goodman, A., Ekker, M., Chevrette, M., Delgado, J., Neuhauss, S., Shimoda, N., Driever, W., Fishman, M. C. and Jacob, H. J.** (1998). A microsatellite genetic linkage map for zebrafish (*Danio rerio*). *Nat. Genet.* **18**, 338-343.
- Kramer, C., Mayr, T., Nowak, M., Schumacher, J., Runke, G., Bauer, H., Wagner, D. S., Schmid, B., Imai, Y., Talbot, W. S. et al.** (2002). Maternally supplied Smad5 is required for ventral specification in zebrafish embryos prior to zygotic Bmp signaling. *Dev. Biol.* **250**, 263-279.
- Larue, L., Ohsugi, M., Hirchenhain, J. and Kemler, R.** (1994). E-cadherin null mutant embryos fail to form a trophectoderm epithelium. *Proc. Natl. Acad. Sci. USA* **91**, 8263-8267.
- Lee, C. H. and Gumbiner, B. M.** (1995). Disruption of gastrulation movements in *Xenopus* by a dominant-negative mutant for C-cadherin. *Dev. Biol.* **171**, 363-373.
- Lele, Z., Folchert, A., Concha, M., Rauch, G. J., Geisler, R., Rosa, F., Wilson, S. W., Hammerschmidt, M. and Bally-Cuif, L.** (2002). parachute/n-cadherin is required for morphogenesis and maintained integrity of the zebrafish neural tube. *Development* **129**, 3281-3294.
- Levine, E., Lee, C. H., Kintner, C. and Gumbiner, B. M.** (1994). Selective disruption of E-cadherin function in early *Xenopus* embryos by a dominant negative mutant. *Development* **120**, 901-909.
- Malicki, J., Jo, H. and Pujic, Z.** (2003). Zebrafish N-cadherin, encoded by the glass onion locus, plays an essential role in retinal patterning. *Dev. Biol.* **259**, 95-108.
- McCrea, P. D., Turck, C. W. and Gumbiner, B.** (1991). A homolog of the armadillo protein in *Drosophila* (plakoglobin) associated with E-cadherin. *Science* **254**, 1359-1361.
- Nagar, B., Overduin, M., Ikura, M. and Rini, J. M.** (1996). Structural basis of calcium-induced E-cadherin rigidification and dimerization. *Nature* **380**, 360-364.
- Reima, I., Lehtonen, E., Virtanen, I. and Flechon, J. E.** (1993). The cytoskeleton and associated proteins during cleavage, compaction and blastocyst differentiation in the pig. *Differentiation* **54**, 35-45.
- Ringwald, M., Baribault, H., Schmidt, C. and Kemler, R.** (1991). The structure of the gene coding for the mouse cell adhesion molecule uvomorulin. *Nucleic Acids Res.* **19**, 6533-6539.
- Rutishauser, U., Acheson, A., Hall, A. and Sunshine, M. J.** (1988). The neural cell adhesion molecule (N-CAM) as a regulator of cell-cell interactions. *Science* **240**, 53-57.
- Sanson, B., White, P. and Vincent, J. P.** (1996). Uncoupling cadherin-based adhesion from wingless signalling in *Drosophila*. *Nature* **383**, 627-630.
- Solnica-Krezel, L., Stemple, D. L., Mountcastle-Shah, E., Rangini, Z., Neuhauss, S. C., Malicki, J., Schier, A. F., Stainier, D. Y., Zwartkruis, F., Abdelilah, S. et al.** (1996). Mutations affecting cell fates and cellular rearrangements during gastrulation in zebrafish. *Development* **123**, 67-80.
- Steinberg, M. S. and Takeichi, M.** (1994). Experimental specification of cell sorting, tissue spreading, and specific spatial patterning by quantitative differences in cadherin expression. *Proc. Natl. Acad. Sci. USA* **91**, 206-209.
- Takeda, H., Simoyama, Y., Nagafuchi, A. and Hirohashi, S.** (1999). E-cadherin functions as a cis-dimer at the cell-cell adhesive interface in vivo. *Nat. Struct. Biol.* **6**, 310-312.
- Takeichi, M.** (1987). Cadherins: a molecular family essential for selective cell-cell adhesion and animal morphogenesis. *Trends Genet.* **3**, 213-217.
- Takeichi, M.** (1995). Morphogenetic roles of classical cadherins. *Curr. Opin. Cell Biol.* **7**, 619-627.
- Thisse, C., Thisse, B., Schilling, T. F. and Postlethwait, J. H.** (1993). Structure of the zebrafish *snail1* gene and its expression in wild-type, *spadetail*, and *no tail* mutants. *Development* **119**, 1203-1215.
- Warga, R. M. and Kane, D. A.** (2003). One-eyed pinhead regulates cell motility independent of Squint/Cyclops signaling. *Dev. Biol.* **261**, 391-411.
- Warga, R. M. and Kimmel, C. B.** (1990). Cell movements during epiboly and gastrulation in zebrafish. *Development* **108**, 569-580.
- Warga, R. M. and Nüsslein-Volhard, C.** (1999). Origin and development of the zebrafish endoderm. *Development* **126**, 827-838.
- Wei, X. and Malicki, J.** (2002). *nagie oko*, encoding a MAGUK-family protein, is essential for cellular patterning of the retina. *Nat. Genet.* **31**, 150-157.
- Westerfield, M.** (1993). *The Zebrafish Book*. Eugene, Oregon: University of Oregon Press.
- Wilson, E. T., Cretokos, C. J. and Helde, K. A.** (1995). Cell mixing during early epiboly in the zebrafish embryo. *Dev. Genet.* **17**, 6-15.